

Isotope shifts and hyperfine structure of the Fe I 372 nm resonance line

S. Krins,¹ S. Opiel,² N. Huet,¹ J. von Zanthier,² and T. Bastin¹

¹*Institut de Physique Nucléaire, Atomique et de Spectroscopie, Université de Liège, 4000 Liège, Belgium*

²*Institut für Optik, Information und Photonik, Universität Erlangen-Nürnberg, 91058 Erlangen, Germany*

(Dated: October 30, 2018)

We report measurements of the isotope shifts of the $3d^6 4s^2 a^5D_4 - 3d^6 4s 4p z^5F_5^o$ Fe I resonance line at 372 nm between all four stable isotopes ^{54}Fe , ^{56}Fe , ^{57}Fe and ^{58}Fe , as well as the complete hyperfine structure of that line for ^{57}Fe , the only stable isotope having a non-zero nuclear spin. The field and specific mass shift coefficients of the transition have been derived from the data, as well as the experimental value for the hyperfine structure magnetic dipole coupling constant A of the excited state of the transition in ^{57}Fe : $A(3d^6 4s 4p z^5F_5^o) = 81.69(86)$ MHz. The measurements were carried out by means of high-resolution Doppler-free laser saturated absorption spectroscopy in a Fe-Ar hollow cathode discharge cell using both natural and enriched iron samples. The measured isotope shifts and hyperfine constants are reported with uncertainties at the percent level.

PACS numbers: 32.10.Fn, 42.62.Fi, 32.30.Jc

I. INTRODUCTION

Isotope shifts and hyperfine splittings of atomic lines and levels are fundamental spectroscopic data playing an important role in many areas of physics and astrophysics, such as in stellar spectroscopic studies [1], in atomic metrology [2] or in cold atom physics [3]. High accuracy laboratory data are needed for a good interpretation of stellar spectra and determination of chemical abundances in stars [4]. This is all the more true for the element iron in view of its fundamental implication in the star evolution process.

In the optical domain, high resolution laser spectroscopy is a very powerful technique to get accurate experimental estimates of isotope shifts and hyperfine splittings. In the case of iron, the energy level structure of the atom has so far prevented an intensive use of this technique since the first excited states need ultraviolet laser radiation to get populated from the ground state (see Ref. [5] for a comprehensive study of the spectrum and level structure of neutral iron). Optical isotope shifts have been reported for five transitions between 300 and 306 nm for the four stable isotopes ^{54}Fe , ^{56}Fe , ^{57}Fe and ^{58}Fe [6]. Laser-Rf double-resonance technique has been successfully used to obtain the hyperfine structure of several metastable states of ^{57}Fe , the only stable isotope having a non-zero nuclear spin $I = 1/2$ [7]. The ground-state configuration hyperfine structure had been measured much earlier very accurately using the atomic beam magnetic resonance technique [8].

More recently, high resolution laser saturated absorption has been observed for the strong resonance line at 372 nm [9] between the ground state $3d^6 4s^2 a^5D_4$ and the odd parity excited state $3d^6 4s 4p z^5F_5^o$ [10]. In that work, a first experimental determination of the isotope shift between the isotopes ^{54}Fe and ^{56}Fe is reported as well as one component of the hyperfine splitting for the isotope ^{57}Fe . The isotope ^{58}Fe is particularly hard to observe because of its very low natural abundance (0.3% [11]).

In this paper, we report the experimental determina-

tion of the isotope shifts of the resonance line at 372 nm between all four stable iron isotopes, as well as the complete hyperfine structure of that line for ^{57}Fe . This allows to propose an experimental value for the hyperfine structure (hfs) magnetic dipole coupling constant A of the excited state $3d^6 4s 4p z^5F_5^o$ along with the specific mass shift and field shift coefficients of the transition. The data were obtained by use of Doppler-free laser saturated absorption [12] on both natural and enriched samples of iron. The paper is organized as follows. In Section II, our experimental setup is described. We then expose our results and their analysis in Section III. We finally draw conclusions in Section IV.

II. EXPERIMENTAL SETUP

The experimental setup is shown in Fig. 1. The radiation at 372 nm was produced by an external cavity diode laser in Littrow design [13] where the first-order diffraction of a grating is coupled back into the laser diode and the output beam is formed by the reflected light of the zeroth order. The linewidth of the laser was less than 1 MHz. The laser frequency was continuously scanned over about 1.5 GHz by means of a Piezo actuator varying the grating angle. A small fraction of the laser beam was sent to a confocal spherical mirror Fabry-Perot interferometer used as a meter to calibrate the frequency scans. The interferometer was installed in a home-made temperature-controlled sealed enclosure and had a free spectral range of 1 GHz with a finesse of about 200. In the experiment, a smaller free spectral range of 107.7(1.1) MHz was deliberately chosen by detuning the mirror separation from the confocal configuration [14]. The corresponding mode spacing was measured by injecting two laser beams into the Fabry-Perot interferometer, shifted in frequency by an acousto-optical modulator, producing a double set of spectra with a fixed and well-known frequency separation.

The main part of the diode laser beam was split into a

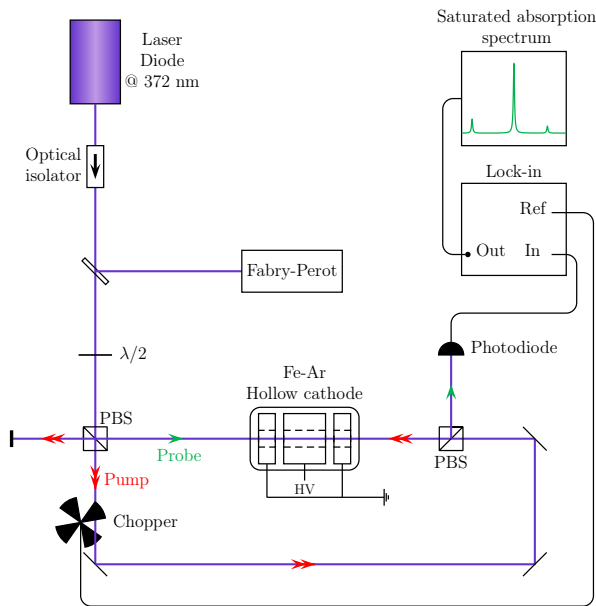


FIG. 1: (Color online) Experimental arrangement used for the observation of Doppler-free saturated absorption spectra of the 372 nm resonance line in neutral iron (see text for an explanation of all elements).

probe and a pump beam by use of a half-wave plate $\lambda/2$ and a polarizing beamsplitter (PBS) for an easy tuning of the relative intensities of the two beams. The counterpropagating beams were overlapped in a home-made cylindrical Fe-Ar hollow cathode with an internal diameter of 8 mm and a length of 50 mm where two aluminum anodes were symmetrically placed on either sides of the cathode at a distance of 1 mm [15]. The pump beam was mechanically chopped while the probe light was registered on a photodiode and further analyzed using a lock-in amplifier referenced to the chopped pump beam. The Doppler-free spectra were directly obtained from the output signal of the lock-in amplifier.

III. RESULTS AND DISCUSSION

A. Spectra

In Fig. 2 we show a typical Doppler-free laser saturated absorption spectrum recorded with a hollow cathode made of natural iron (5.8% of ^{54}Fe , 91.8% of ^{56}Fe , 2.1% of ^{57}Fe and 0.3% of ^{58}Fe [11]). The strong central line corresponds to the transition $3d^6 4s^2 a^5 D_4 - 3d^6 4s 4p z^5 F_5^o$ Fe I transition at 372 nm for the most abundant isotope ^{56}Fe in the sample. The lower frequency line is the same transition for the isotope ^{54}Fe . Towards the higher frequencies after the central line, the next two small lines are two hyperfine components of the ^{57}Fe transition, while the final weak line is the ^{58}Fe contribution. The hyperfine structure of

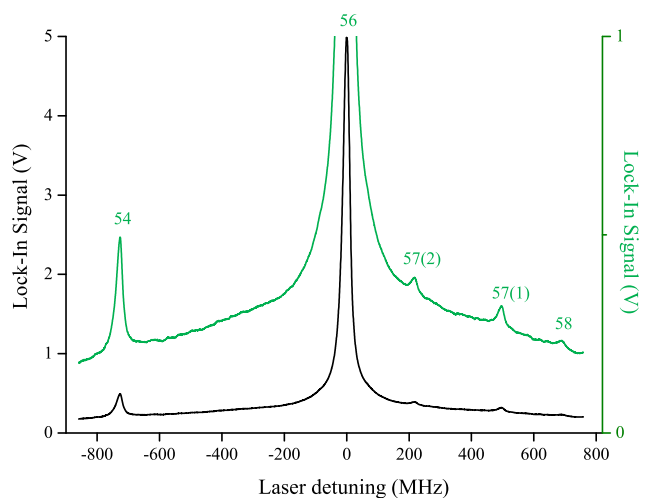


FIG. 2: (Color online) Typical Doppler-free laser saturated absorption spectrum recorded with a hollow cathode made of natural iron, illustrated on two different scales. All lines refer to the $3d^6 4s^2 a^5 D_4 - 3d^6 4s 4p z^5 F_5^o$ Fe I transition at 372 nm [9] for the different stable isotopes ^{54}Fe , ^{56}Fe , ^{57}Fe and ^{58}Fe . The isotope ^{57}Fe is the only one to possess a hyperfine structure. Two hyperfine components of the investigated transition are visible in the present spectrum (denoted (1) and (2) in decreasing order of intensity). As expected, a third hyperfine component predicted more than 50 times weaker than the first component is not visible. The frequency axis is referenced with respect to the central ^{56}Fe peak.

the ^{57}Fe transition is illustrated in Fig. 3. The lower [upper] level is split into two hyperfine levels $F = 9/2$ and $F = 7/2$ [$F = 11/2$ and $F = 9/2$] that are shifted with respect to their unperturbed fine structure level by the amount $AC/2$ with A the hfs magnetic dipole coupling constant of the unperturbed level and

$$C = F(F + 1) - I(I + 1) - J(J + 1), \quad (1)$$

with F, I and J the total angular momentum, nuclear spin and total electronic angular momentum quantum numbers, respectively. No electric quadrupole effect is present in ^{57}Fe because of the nucleus spherical symmetry ($I = 1/2$). The level splitting of the investigated transition gives rise to three hfs line components $9/2 - 11/2$, $7/2 - 9/2$ and $9/2 - 9/2$, with theoretical relative intensities of $100 : 81.5 : 1.9$ [16], hereafter simply denoted by (1), (2) and (3), respectively. As expected, the weakest hfs component is not observed in the spectrum of Fig. 2. Indirect observations of this last component were obtained using enriched samples of iron. This is shown in Fig. 4 with a typical spectrum recorded with a copper hollow cathode covered with a few milligrams of a home-made iron powder containing approximately 10% of ^{54}Fe , 10% of ^{56}Fe , 70% of ^{57}Fe , and 10% of ^{58}Fe . In comparison with the spectrum of Fig. 2, the three lines of the even isotopes here have an approximately equal intensity, while all hfs components of the ^{57}Fe isotope

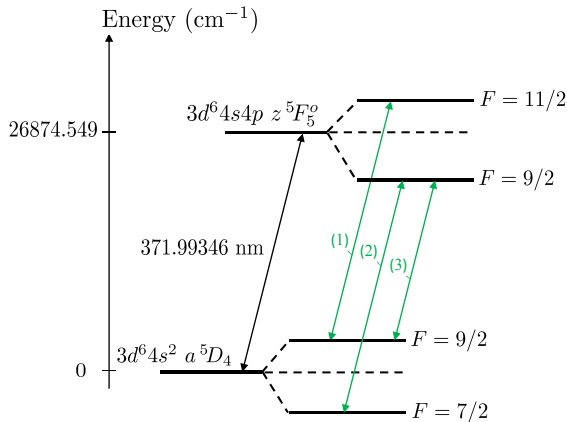


FIG. 3: (Color online) Hyperfine structure components (1), (2) and (3) of the $3d^6 4s^2 a^5 D_4 - 3d^6 4s 4p z^5 F_5^0$ Fe I transition at 372 nm for the isotope ^{57}Fe (nuclear spin $I = 1/2$). The quoted excited state energy and air wavelength of the transition are the accurate values of Ref. [5].

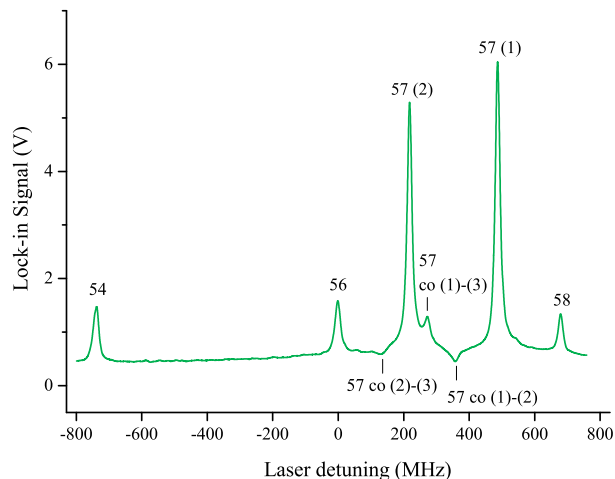


FIG. 4: (Color online) Same Doppler-free laser saturated absorption spectrum as in Fig. 2 recorded with an enriched sample of iron ($\approx 10\%$ ^{54}Fe , $\approx 10\%$ ^{56}Fe , $\approx 70\%$ ^{57}Fe , and $\approx 10\%$ ^{58}Fe). In addition to the lines observed in Fig. 2, all cross-over (co) resonances between the ^{57}Fe hyperfine components are visible in the spectrum.

are significantly enhanced in accordance with the chosen isotope abundances in the sample. In addition to the lines observed in Fig. 2, all cross-over (co) resonances [18] between the ^{57}Fe hfs components are visible in the spectrum. The cross-over resonances between hfs components (1) and (2), and (2) and (3) are inverted. The clearly visible cross-over signal between hfs components (1) and (3) yielded a good indirect observation of component (3).

IS (MHz)	$\delta\nu_{58,56}$	$\delta\nu_{57,56}$	$\delta\nu_{56,54}$
Ref. [10]	—	—	725(10)
This work	689.9(7.3)	365.1(5.7)	726.5(7.7)

TABLE I: Isotope shifts (IS) between the given iron isotopes for the Fe I 372 nm resonance line.

A (MHz)	$3d^6 4s^2 a^5 D_4$	$3d^6 4s 4p z^5 F_5^0$
Ref. [8]	38.0795(10)	—
This work	38.33(40)	81.69(86)

TABLE II: Hyperfine structure magnetic dipole coupling constants A of the lower and upper levels of the Fe I 372 nm resonance line.

B. Isotope shifts and hyperfine structure constants

The peak frequencies $\nu_{54}, \nu_{56}, \nu_{57(1)}, \nu_{57(2)}, \nu_{57(3)}$ and ν_{58} allow us to determine all isotope shifts and the hfs magnetic dipole coupling constants of both ground and excited states for ^{57}Fe . Due to the absence of nuclear spin, the isotope shifts $\delta\nu_{56,54}$ and $\delta\nu_{58,56}$ are simply given by $\nu_{56} - \nu_{54}$ and $\nu_{58} - \nu_{56}$, respectively. For ^{57}Fe , the isotopic and hyperfine structure effects are intertwined. The isotope shift $\delta\nu_{57,56}$ is the line frequency shift that would be observed between isotopes 57 and 56 without nuclear magnetic effects. In their presence, all effects add up and we do have for each hfs component $i = 1, 2, 3$

$$\nu_{57(i)} - \nu_{56} = \delta\nu_{57,56} + \frac{1}{2}A'C'_{(i)} - \frac{1}{2}AC_{(i)}, \quad (2)$$

with A [A'] and $C_{(i)}$ [$C'_{(i)}$] the hfs magnetic dipole coupling constant and the constant of Eq. (1) for the lower [upper] level of the hyperfine component (i), respectively. Inverting Eq. (2) yields directly $\delta\nu_{57,56}$, A and A' from the three frequency shifts $\nu_{57(i)} - \nu_{56}$ ($i = 1, 2, 3$).

To get a representative sample of experimental results, 24 spectra similar to Fig. 4 were recorded, all with typical cathode currents of about 200 mA and an argon gas pressure of 0.3 mbar. The pump and probe beam intensities were typically 70 mW/cm² and 8 mW/cm², respectively. Under those experimental conditions, the recorded lines had a linewidth of about 17 MHz. This value originates from the 2.59(2) MHz natural linewidth [17], power broadened up to about 9 MHz in view of the saturation intensity of the line (6.57(4) mW/cm²). The last 8 MHz contribution to the observed linewidth is attributed to collisional broadening not completely negligible at the pressure the hollow cathode cell was operated.

Tables I and II summarize our experimental data. The errors quoted represent the statistical errors (one standard deviation of the mean of the sample of 24 spectra) combined with an uncertainty of 1% in the determination of the Fabry-Perot free spectral range. The isotope

shifts $\delta\nu_{57,56}$ and $\delta\nu_{58,56}$ have been determined for the first time, as well as the hfs magnetic dipole coupling constant A of the excited state. The other data are in very good agreement within experimental uncertainties with respect to previously reported values. In Ref. [10], the shift between the hfs component (1) of ^{57}Fe and the ^{56}Fe peak is reported to be equal to 495(10) MHz; in excellent agreement we obtained the result 492.7(5.2) MHz. The uncertainties of the ground state hfs constants A obtained in this work and in Ref. [8] cannot be compared since the present optical method is simply not able to compete with radio-frequency techniques. On the other hand, optical methods offer access to levels otherwise inaccessible with radio-frequency techniques, as is the case with the excited level investigated in this paper.

C. Field and specific mass shifts

As is well known, the frequency shift $\delta\nu_{A,A'}$ of a transition between two isotopes of mass A and A' can be expressed as [19]

$$\delta\nu_{A,A'} = k\mu_{A,A'}^{-1} + F\delta\langle r^2 \rangle_{A,A'}, \quad (3)$$

where k and F are the mass and field shift coefficients of the transition, respectively, $\delta\langle r^2 \rangle_{A,A'}$ is the difference in mean square nuclear charge radii between the two isotopes, and $\mu_{A,A'} = AA'/(A - A')$. The mass shift coefficient k is the sum of two contributions, the normal mass shift coefficient k_{NMS} and the specific mass shift coefficient k_{SMS} : $k = k_{\text{NMS}} + k_{\text{SMS}}$. The normal mass shift coefficient takes the reduced mass correction for the electron into account and amounts to $\nu m_e/u$ with ν the transition frequency, m_e the electron mass and u the atomic mass unit. The specific mass shift originates from the change in the correlated motion of all the electrons and is much more difficult to evaluate accurately from *ab initio* theoretical calculations. Subtraction of the normal mass shift from the isotope shift $\delta\nu_{A,A'}$ gives the residual isotope shift $\delta\nu_{A,A'}^{\text{RIS}}$, verifying

$$\mu_{A,A'}\delta\nu_{A,A'}^{\text{RIS}} = k_{\text{SMS}} + F\mu_{A,A'}\delta\langle r^2 \rangle_{A,A'}. \quad (4)$$

Equation (4) shows that the so-called King's plot [19] of the modified residual isotope shift $\mu_{A,A'}\delta\nu_{A,A'}^{\text{RIS}}$, as a function of the modified difference in mean square nuclear charge radii $\mu_{A,A'}\delta\langle r^2 \rangle_{A,A'}$ for different isotope pairs draws a straight line of slope F and with origin value k_{SMS} .

In Fig. 5 we show the King's plot drawn from our measured isotope shifts reported in Table I and with $\delta\langle r^2 \rangle_{A,A'}$ values deduced from tabulated rms nuclear charge radii measured by electron scattering and muonic x rays [20]. The linear regression of the plotted points has allowed for the first time to obtain an experimental value for the specific mass shift and field shift coefficients of the Fe I

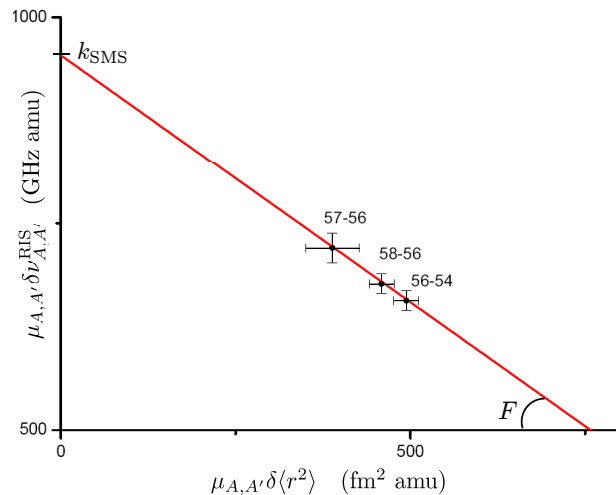


FIG. 5: (Color online) King's plot of the modified residual isotope shift $\mu_{A,A'}\delta\nu_{A,A'}^{\text{RIS}}$ with respect to the modified difference in mean square nuclear charge radii $\mu_{A,A'}\delta\langle r^2 \rangle_{A,A'}$ for the different isotope pairs 58–56, 57–56 and 56–54. The origin value and slope of the linear regression line yield the specific mass shift k_{SMS} and field shift F coefficients, respectively.

372 nm resonance transition, namely

$$\begin{aligned} k_{\text{SMS}} &= 950(140) \text{ GHz amu}, \\ F &= -0.60(31) \text{ GHz/fm}^2. \end{aligned} \quad (5)$$

These values allow in turn to compute the contribution of the specific mass shift $k_{\text{SMS}}\mu_{A,A'}^{-1}$ and the field shift $F\delta\langle r^2 \rangle_{A,A'}$ for each measured isotope shifts between two isotopes of mass A and A' . These contributions are summarized in Table III for our data. As can be seen, the major contribution to the residual isotope shifts comes from the specific mass shift term. It must be noted that the uncertainties quoted in Eq. (5) originate mainly from the nuclear rms charge radius errors [20] that contribute to the standard deviations of the coefficients k_{SMS} and F by 110 GHz amu and 0.23 GHz/fm², respectively. This shows that no significant reduction of the uncertainties of these coefficients can be expected without a more accurate determination of the nuclear charge radii.

It is worth mentioning that the specific mass shift coefficient was estimated to be $k_{\text{SMS}} = 734$ GHz amu in a recent theoretical study [21]. This value is lower than our experimental result by 1.5 standard deviations.

IV. CONCLUSION

In conclusion, in this paper we have reported the experimental determination of the isotope shifts of the $3d^6 4s^2 a^5 D_4 - 3d^6 4s 4p z^5 F_5^o$ Fe I resonance line at 372 nm between all four stable isotopes ^{54}Fe ($I = 0$), ^{56}Fe ($I = 0$), ^{57}Fe ($I = 1/2$), and ^{58}Fe ($I = 0$), as well as the

Isotope pair	IS (MHz)	RIS (MHz)	SMS (MHz)	FS (MHz)
58 – 56	689.9(7.3)	417.3(7.3)	587(87)	–169(88)
57 – 56	365.1(5.7)	226.3(5.7)	299(44)	–73(38)
56 – 54	726.5(7.7)	434.2(7.7)	629(93)	–200(100)

TABLE III: Isotope shift (IS), residual isotope shift (RIS), specific mass shift (SMS) and field shift (FS) between the given isotopes for the Fe I 372 nm resonance line.

complete hyperfine structure of that line for ^{57}Fe . The measurements were made using high-resolution Doppler-free laser saturated absorption spectroscopy in a homemade Fe-Ar hollow cathode discharge cell with both natural and enriched iron samples. The measured isotope shifts and hyperfine constants have been reported with uncertainties at the percent level. The frequency shifts $\delta\nu_{57,56}$ and $\delta\nu_{58,56}$ have been reported for the first time,

as well as the experimental value for the hyperfine structure magnetic dipole coupling constant A of the excited state of the transition. The field and specific mass shift coefficients of the transition have been derived from a King’s plot analysis where it was shown that the major part of the measured isotope shifts comes from the specific mass shift contribution.

Acknowledgments

T.B. and S.K. thank the Belgian F.R.S.-FNRS and Institut Interuniversitaire des Sciences Nucléaires for financial support. The authors would like to thank N. Krins for her assistance in the chemical preparation of the enriched iron powder, R. Maiwald and A. Golla for their experimental support in the Fabry-Perot calibration measurements, E. Biémont, G. Haesbroeck, M. Godefroid, G. H. Guthöhrlein, and P. Quinet for helpful discussions, and H.-P. Garnir for financial support.

-
- [1] R. L. Kurucz, *Physica Scripta* **T47**, 110 (1993).
 - [2] T. Rosenband *et al.*, *Science* **319** 1808 (2008).
 - [3] W. D. Phillips, *Rev. Mod. Phys.* **70**, 721 (1998).
 - [4] D. Leckrone, S. Johansson, G. M. Wahlgren, C. R. Profitt, and T. Brage, *Physica Scripta* **T65**, 110 (1996).
 - [5] H. M. Crosswhite, *J. Res. Natl. Bur. Stand. (US)* **79A**, 17 (1975).
 - [6] D. M. Benton, E. C. A. Cochrane, and J. A. R. Griffith, *J. Phys. B: At. Mol. Opt. Phys.* **30**, 5359 (1997).
 - [7] J. Dembczyński, W. Ertmer, U. Johann, and P. Stinner, *Z. Physik A* **294**, 313 (1980); W. Ertmer, U. Johann, J. Dembczyński, and Z. Michalski, *Z. Phys. D* **2**, 67 (1986).
 - [8] W. J. Childs, and L. S. Goodman, *Phys. Rev.* **148**, 74 (1966).
 - [9] The air wavelength reads accurately 371.99346 nm [5].
 - [10] B. Smeets, R. C. M. Bosch, P. Van Der Straten, E. Te Sligte, R. E. Scholten, H. C. W. Beijerinck, and K. A. H. Van Leeuwen, *Appl. Phys. B* **76**, 815 (2003).
 - [11] K. J. R. Rosman and P. D. P. Taylor, *Pure & Appl. Chem.* **70**, 217 (1998).
 - [12] T. Hänsch, M. D. Levenson, and A. L. Schawlow, *Phys. Rev. Lett.* **26**, 946 (1971).
 - [13] L. Ricci, M. Weidemüller, T. Esslinger, A. Hemmerich, C. Zimmermann, V. Vuletic, W. König, and T. W. Hänsch, *Opt. Commun.* **117**, 541 (1995).
 - [14] K. Kerner, S. M. Rochester, V. V. Yashchuk, and D. Budker, [arXiv:physics/0306144](https://arxiv.org/abs/physics/0306144).
 - [15] P.-H. Lefèbvre, H.-P. Garnir, and E. Biémont, *Phys. Scr.* **66**, 363 (2002).
 - [16] I. I. Sobelman, *Atomic Spectra and Radiative Transitions* (Nauka, Moscow, 1977; Springer, Berlin, 1999).
 - [17] J. Z. Klose, *Astron. Astrophys.* **165**, 637 (1971).
 - [18] H. K. Holt, *Phys. Rev. Lett.* **29**, 1138 (1972).
 - [19] W. H. King, *Isotope Shifts in Atomic Spectra* (Plenum Press, New York/London, 1984).
 - [20] I. Angeli, *At. Data Nucl. Data Tables* **87**, 185 (2004).
 - [21] S. G. Porsev, M. G. Kozlov, and D. Reimers, *Phys. Rev. A* **79**, 032519 (2009).